

Article

Development of a Flash Drought Intensity Index

Jason A. Otkin ^{1,*}, Yafang Zhong ¹, Eric D. Hunt ², Jordan I. Christian ³, Jeffrey B. Basara ^{3,4},
Hanh Nguyen ⁵, Matthew C. Wheeler ⁵, Trent W. Ford ⁶, Andrew Hoell ⁷, Mark Svoboda ⁸
and Martha C. Anderson ⁹

- ¹ Space Science and Engineering Center, Cooperative Institute for Meteorological Satellite Studies, University of Wisconsin-Madison, Madison, WI 53706, USA; yafangzhong@wisc.edu
- ² Atmospheric and Environmental Research, Inc., Lexington, MA 02421, USA; ehunt@aer.com
- ³ School of Meteorology, University of Oklahoma, Norman, OK 73702, USA; jchristian@ou.edu (J.I.C.); jbasara@ou.edu (J.B.B.)
- ⁴ School of Civil Engineering and Environmental Science, University of Oklahoma, Norman, OK 73702, USA
- ⁵ Bureau of Meteorology, Melbourne, VIC 3008, Australia; hanh.nguyen@bom.gov.au (H.N.); matthew.wheeler@bom.gov.au (M.C.W.)
- ⁶ Illinois Water Survey, University of Illinois, Champaign, IL 61820, USA; twford@illinois.edu
- ⁷ Physical Sciences Laboratory, National Oceanic and Atmospheric Administration, Boulder, CO 80305, USA; andrew.hoell@noaa.gov
- ⁸ National Drought Mitigation Center, University of Nebraska, Lincoln, NE 68583, USA; msvoboda2@unl.edu
- ⁹ Agricultural Research Service, Hydrology and Remote Sensing Laboratory, United States Department of Agriculture, Beltsville, MD 20705, USA; martha.anderson@usda.gov
- * Correspondence: jasono@ssec.wisc.edu



Citation: Otkin, J.A.; Zhong, Y.; Hunt, E.D.; Christian, J.I.; Basara, J.B.; Nguyen, H.; Wheeler, M.C.; Ford, T.W.; Hoell, A.; Svoboda, M.; et al. Development of a Flash Drought Intensity Index. *Atmosphere* **2021**, *12*, 741. <https://doi.org/10.3390/atmos12060741>

Academic Editors: Muthuvel Chelliah and Lifeng Luo

Received: 7 May 2021

Accepted: 5 June 2021

Published: 9 June 2021

Publisher's Note: MDPI stays neutral with regard to jurisdictional claims in published maps and institutional affiliations.



Copyright: © 2021 by the authors. Licensee MDPI, Basel, Switzerland. This article is an open access article distributed under the terms and conditions of the Creative Commons Attribution (CC BY) license (<https://creativecommons.org/licenses/by/4.0/>).

Abstract: Flash droughts are characterized by a period of rapid intensification over sub-seasonal time scales that culminates in the rapid emergence of new or worsening drought impacts. This study presents a new flash drought intensity index (FDII) that accounts for both the unusually rapid rate of drought intensification and its resultant severity. The FDII framework advances our ability to characterize flash drought because it provides a more complete measure of flash drought intensity than existing classification methods that only consider the rate of intensification. The FDII is computed using two terms measuring the maximum rate of intensification (FD_INT) and average drought severity (DRO_SEV). A climatological analysis using soil moisture data from the Noah land surface model from 1979–2017 revealed large regional and interannual variability in the spatial extent and intensity of soil moisture flash drought across the US. Overall, DRO_SEV is slightly larger over the western and central US where droughts tend to last longer and FD_INT is ~75% larger across the eastern US where soil moisture variability is greater. Comparison of the FD_INT and DRO_SEV terms showed that they are strongly correlated ($r = 0.82$ to 0.90) at regional scales, which indicates that the subsequent drought severity is closely related to the magnitude of the rapid intensification preceding it. Analysis of the 2012 US flash drought showed that the FDII depiction of severe drought conditions aligned more closely with regions containing poor crop conditions and large yield losses than that captured by the intensification rate component (FD_INT) alone.

Keywords: flash drought; drought; soil moisture; crop yield; climate; climate extreme; land surface model; United States of America

1. Introduction

Flash droughts are characterized by unusually rapid intensification over sub-seasonal time scales that culminates in drought conditions [1]. A seminal study by Otkin et al. (2013) [2] revealed that rapid increases in moisture stress during flash drought are often accompanied by extreme heat, reduced cloud cover, low relative humidity, and strong winds. Ford and Labosier (2017) [3] found that variables depicting anomalies in atmospheric evaporative demand or the balance between the supply and demand of surface moisture are closely related to flash drought onset. The co-occurrence of below normal precipitation

and elevated evaporative demand can lead to the rapid depletion of root zone soil moisture due to the dual impacts of increased evapotranspiration and diminished recharge of soil moisture [2,4]. This in turn can lead to a rapid increase in vegetation moisture stress and the emergence of flash drought conditions [5–8]. Flash drought is a compound extreme climate event characterized by a combination of drivers and hazards that contribute to societal and environmental risks [9].

Because flash drought is more likely to occur during the growing season when evaporative demand is high [10], it can lead to sharply lower crop yields and damage to natural ecosystems [11–13]. For example, a rapid transition toward severe drought across the southeastern US in the fall of 2016 led to numerous wildfires, most notably represented by the devastating fires near Gatlinburg, Tennessee in late November [14]. Likewise, the extreme flash drought that occurred during 2012 across prime agricultural lands in the central US led to losses in excess of \$30 billion [15]. Another example is the 2010 flash drought across Russia and Ukraine that led the Russian government to ban the export of wheat. This decision had national security implications because subsequent increases in bread prices may have played a role in the protests and uprisings that occurred during the Arab Spring in 2011 [16]. These and other examples illustrate the adverse effects that flash droughts have on the environment and economy [17–24].

The high impact of flash drought has motivated development of various methods to identify these features in the historical record and as part of real-time monitoring applications. Most studies have identified flash drought based on the presence of unusually rapid changes in the ratio of actual to potential evapotranspiration [2,21,25,26], soil moisture [3,7,27–29], evaporative demand [30,31], water balance [32], or the US Drought Monitor (USDM) [33–35] over several weeks. These variables are typically chosen because they capture the main drivers and impacts of moisture-related vegetation stress. Most of the studies identify flash drought using a set of thresholds requiring a minimum rate of intensification over a certain period of time [36]. These definitions are consistent with recommendations in the flash drought review article by Otkin et al. (2018) [1]; however, most are unable to quantify the intensity of the flash drought. Two exceptions are Christian et al. (2019) [25] and Li et al. (2020) [26], both of which categorize flash droughts based on the magnitude of their rapid intensification.

Though existing flash drought definitions capture the rapid intensification component, they do not consider the actual drought severity during or after the rapid intensification period. This is a critical omission because land surface and hydrologic impacts will be closely related not only to how quickly drought conditions develop but also by how severe they become. A natural question is whether noteworthy flash droughts would have been considered exceptionally severe had their rapid intensification been terminated by heavy rainfall that quickly ameliorated drought conditions. For example, though people were caught by surprise by the extremely rapid drought intensification that occurred during the 2012 and 2017 US flash droughts [37,38], what made them especially destructive was that the extreme drought conditions persisted for many months after the period of rapid intensification ended. These examples illustrate why it is important to consider both the magnitude of the rapid intensification and the resultant drought severity when assessing flash drought characteristics. Christian et al. (2019) [10] and Liu et al. (2020) [24] have partially addressed this limitation by identifying cases where flash droughts transitioned into hydrological or seasonal droughts; however, neither study combined the rapid intensification and severity components into a single metric.

In this study, we develop a new flash drought intensity index (FDII) that explicitly accounts both for the rapid rate of intensification of a flash drought and the resultant drought severity. This is an important development for flash drought monitoring and research because it provides a more complete measure of flash drought severity than existing identification methods that focus only on the rate of intensification. Development of the FDII will aid efforts to characterize these extreme climate events and the impacts they have on agriculture and natural ecosystems [39–42]. It will also be valuable for quantifying

trends not only in flash drought occurrence [29,43], but also in their intensity, both in the historical record and in the future under different climate scenarios [44]. The FDII could also assist climate and climate change vulnerability assessments by providing a new index that would allow researchers to investigate environmental and socioeconomic impacts associated with flash droughts of varying intensity [45–47]. As a biophysical indicator of drought intensity, the FDII could serve as the basis for biophysical, socioeconomic, or integrated vulnerability assessment studies [48–50]. As such, there are various potential applications for the FDII methodology.

2. Materials and Methods

2.1. Soil Moisture

The FDII methodology will be demonstrated using soil moisture output from the Noah land surface model [51] from the North American Land Data Assimilation System [52]. Soil moisture from the 0–40 cm layer is chosen for this analysis as a balance between the rapid (but noisy) response of topsoil moisture and the slower evolution of soil moisture in deeper layers. Hourly soil moisture values with 0.125° spatial resolution were averaged to pentads (5 days) and then percentiles were computed using the climatological soil moisture distribution from 1979–2017. This process was applied separately to each pentad and grid point to account for seasonal and local differences in the soil moisture climatology. Verification studies have shown that Noah soil moisture data exhibit high fidelity when compared to in situ observations [52,53].

2.2. Flash Drought Intensity Index (FDII)

The FDII includes two components: one that measures the rate of intensification (FD_INT) and a second that captures the drought severity (DRO_SEV). We refer to this index as the “FD-two” because it considers both components when assessing the intensity of flash drought. Here, we provide an example where the FDII is computed using percentiles, though standardized change anomalies could also be used. The intensification and severity components are computed relative to baseline values that represent the minimum requirements for flash drought. For this study, we require a minimum intensification rate equivalent to a 15 percentile decrease (ΔPER_BASE) in soil moisture during a 4-pentad period (ΔT_BASE), which is similar to thresholds used in previous studies to identify flash drought [3,27]. The flash drought intensification component (FD_INT) for a given pentad is computed as:

$$FD_INT = \left(\frac{\Delta PER_BASE}{\Delta T_BASE} \right)^{-1} \times \left(\frac{\Delta PER_OBS}{\Delta T_OBS} \right)_{\max} \quad (1)$$

where the first term is a constant representing the inverse of the baseline minimum intensification rate and the second term is the maximum observed intensification rate. The latter term is computed by sequentially searching for the maximum intensification rate occurring over time periods ranging from 2 to 10 pentads ending at the analysis time. This time range was chosen because flash drought is a sub-seasonal phenomenon. Using a variable time range allows the FDII framework to capture the maximum intensification rate for each event, which may occur over different time scales due to differences in antecedent conditions and the processes driving the evolution of the flash drought. When scaled by the baseline intensification rate, this means that the percentile changes required for an event to be classified as a flash drought increases with time, ranging from a minimum intensification rate of a 7.5 percentile decrease in 2 pentads to a 37.5 percentile decrease in 10 pentads. FD_INT is set to zero for pentads that do not meet the baseline intensification rate requirement. This flexible framework allows us to not only identify flash drought, but also to assess its intensity. For example, Figure 1a shows the evolution of two hypothetical flash drought events where event 2 has a larger FD_INT on 5 June than event 1 because it was characterized by a larger percentile decrease over a shorter period of time preceding this date.

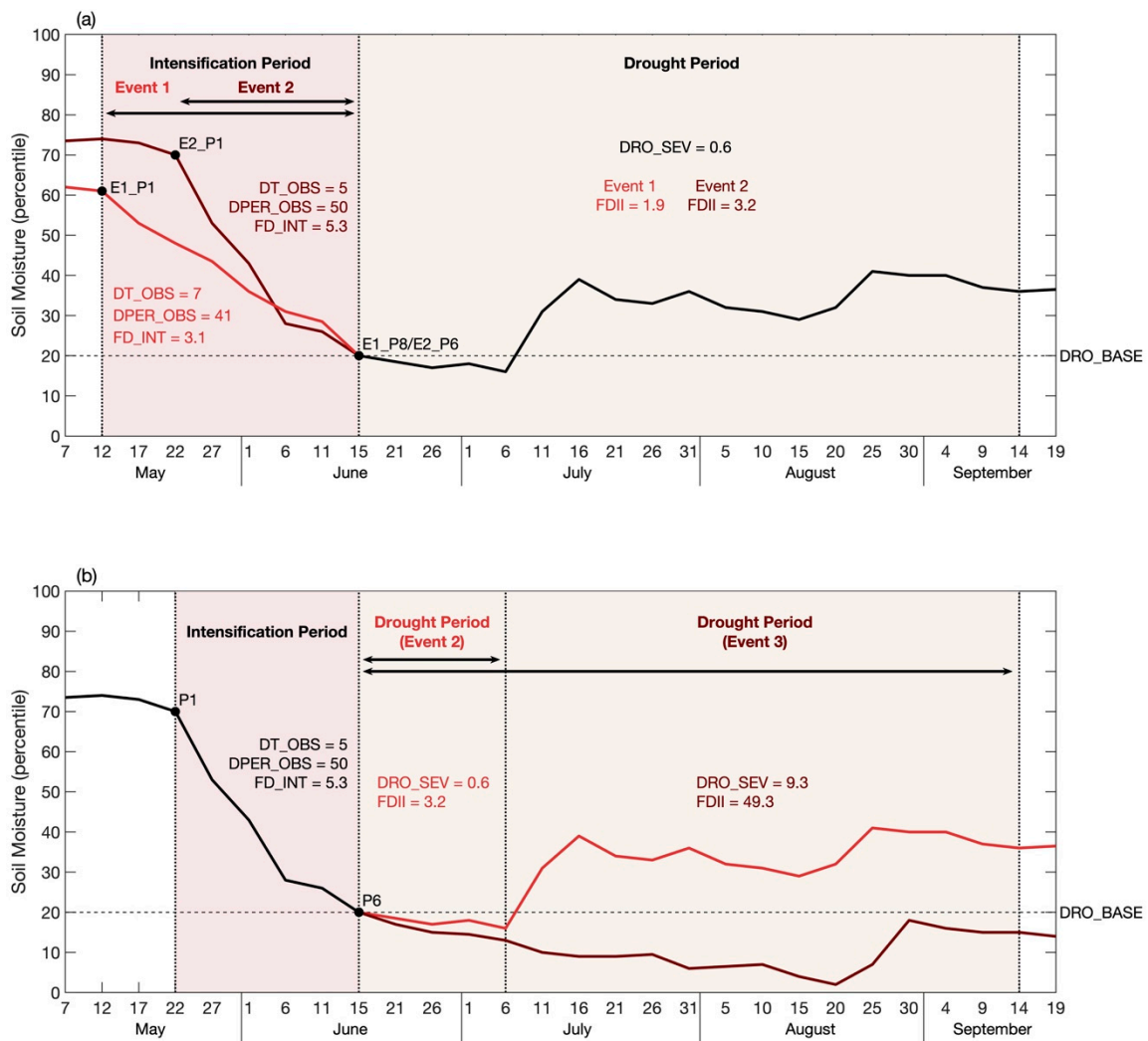


Figure 1. Examples illustrating how differences in the (a) rate of intensification (FD_INT) and (b) drought severity (DRO_SEV) for three hypothetical flash drought events modulate the magnitude of the FDII.

After computing the FD_INT term, it is then necessary to determine the drought severity (DRO_SEV) associated with the flash drought. Here, we choose to compute the average drought severity during the 18 pentads (90 days) following the end of the rapid intensification period:

$$DRO_SEV = \frac{1}{np} \sum_{n=1}^{np} (DRO_BASE - DRO_OBS(n)) \quad (2)$$

where np is the number of pentads, $DRO_OBS(n)$ is the observed percentile for pentad n , and DRO_BASE is the baseline percentile threshold used to represent the onset of drought conditions. We require that the variable must fall below the 20th percentile of its distribution ($DRO_BASE = 20$) [33] for at least four consecutive pentads for it to be considered a flash drought. If $DRO_OBS(n) > DRO_BASE$ for an individual pentad, the drought severity is set to zero for that pentad. This approach is advantageous because it allows us to consider drought severity over a range of time scales (but limited in duration by np), with the DRO_SEV term becoming larger the longer drought conditions last. It also permits temporary improvements above DRO_BASE within the time period used to compute DRO_SEV.

Finally, the FDII is then computed as the product of the FD_INT and DRO_SEV components so that the intensification rate and actual drought severity can be considered in a combined flash drought analysis framework:

$$\text{FDII} = \text{FD_INT} \times \text{DRO_SEV} \quad (3)$$

The importance of accounting for the drought severity when assessing flash drought is illustrated in Figure 1b for two events that have identical intensification rates ($\text{FD_INT} = 5.3$) but then have different evolutions after the period of rapid intensification ends. In this example, event 3 has a larger FDII than event 2 because the drought conditions were more severe and lasted longer.

3. Results

3.1. Flash Drought Climatology

In this section, we explore regional and seasonal differences in flash drought characteristics when the FDII framework is applied to the Noah soil moisture dataset. Figure 2 shows the average FD_INT, DRO_SEV, and FDII for each grid point at monthly intervals during the primary growing season (April to October), along with the percentage of pentads for which flash drought occurred during each month in the climatology. Only pentads containing flash drought were used to compute the average values for each term, with a given pentad identified as containing flash drought if the intensification rate exceeded the minimum intensification rate and the soil moisture percentile was at or below *DRO_BASE* for the current and next three pentads.

Inspection of the percentage time column reveals that soil moisture flash droughts can develop throughout the growing season but occur most frequently during the summer and fall when evaporative demand and vegetation water requirements are high. Large regional differences in flash drought occurrence are also evident. For example, flash droughts develop most often in June and July across the northwestern US, the summer in the central US, and the fall across the southern US. The seasonal peak across the central US is broadly consistent with the study by Christian et al. (2019) [10] that used rapid changes in the ratio of actual to potential evapotranspiration to identify flash droughts over a 38-year period. The similar seasonal distributions of flash drought occurrence across the central US when using soil moisture or evapotranspiration-based metrics could be due to stronger land–atmosphere coupling in this region [54–58].

Figure 2 demonstrates notable differences in spatial patterns and seasonality between the FD_INT and DRO_SEV terms. For example, most areas characterized by large FD_INT in any given month also had fewer flash droughts and smaller average DRO_SEV than elsewhere. This relationship is most prominent across portions of the Midwest, New England, and the southeastern US. This indicates that though drought intensification can be very rapid in these locations, it does not occur as often, and severe or persistent drought conditions are less likely to develop after the period of rapid intensification ends. This pattern is consistent with the tendency for the eastern US. to have more reliable rainfall and lower evaporative demand, both of which make it less likely that a period of rapid intensification will transition into long-term severe drought. FD_INT is largest across the eastern US whereas DRO_SEV is largest across the western and central US, where droughts are more likely to persist for many weeks or months. Together, this leads to larger average FDII values in the central and western US than would occur if only the magnitude of the rapid intensification was used to depict their severity.

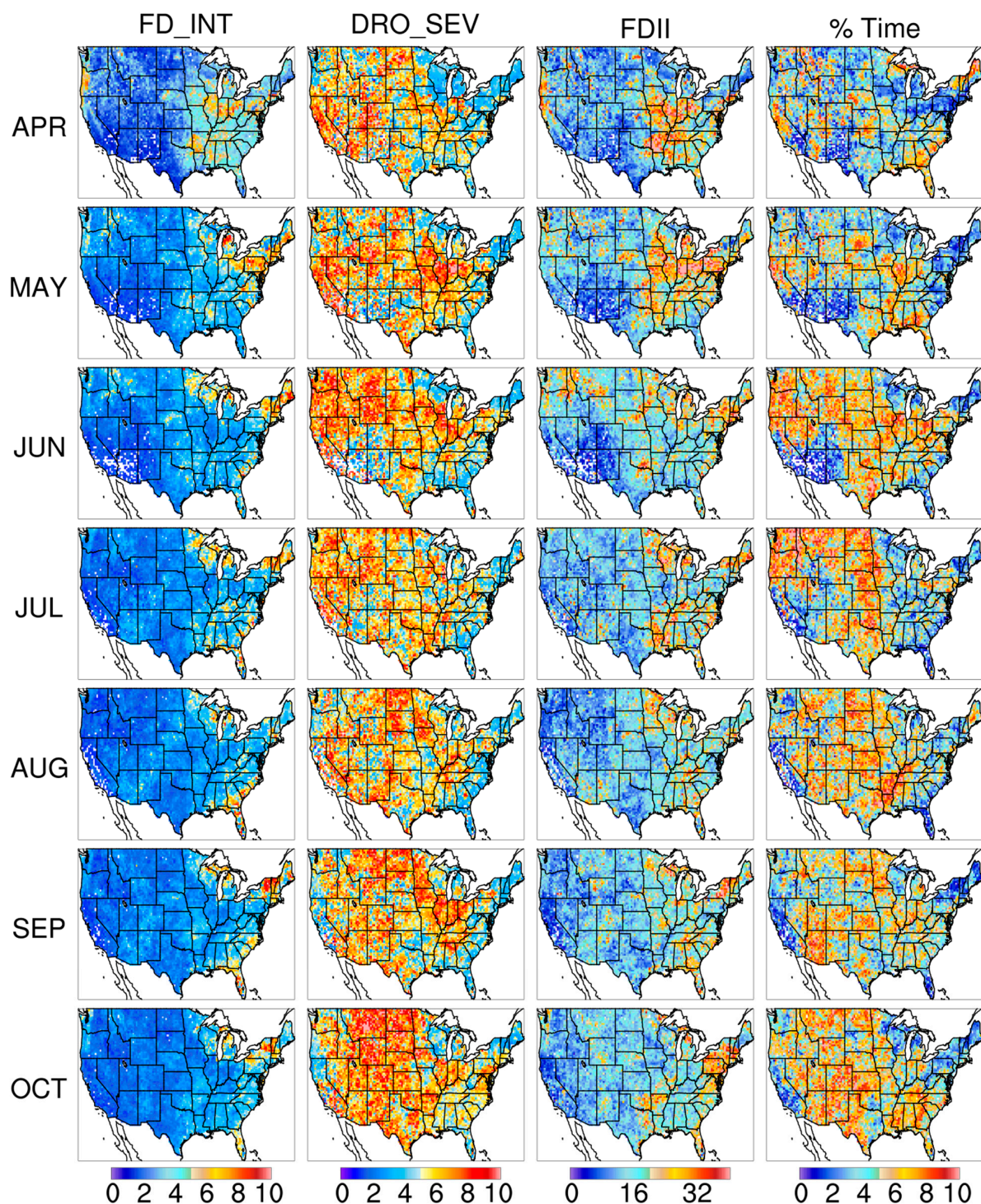


Figure 2. Monthly climatology depicting the average (left column) FD_INT, (second column) DRO_SEV, and (third column) FDII for each grid point, and the (right column) percentage of pentads characterized by flash drought during the 1979–2017 period of record. Only pentads containing flash drought were used to compute the values for each term.

Figure 3 shows probability distributions for FDII, FD_INT, and DRO_SEV for six regions in the US, along with the mean value for each distribution, generated using values from individual pentads and grid points for which flash drought occurred during 1979–2017. These regions were chosen based on the longitudinal distribution of flash droughts shown in Figure 2 and to account for differences in climate between cooler northern areas and warmer southern parts of the US. Comparison of the distributions reveals

large variations in flash drought characteristics from west to east across the US, with smaller differences between the northern and southern regions. For example, FD_INT distributions (Figure 3c) in the western regions show a strong peak near 1.5, whereas the eastern regions show flatter distributions characterized by a smaller peak near 2.5 and higher probabilities of FD_INT > 3. The rightward shift causes the average FD_INT to be ~75% larger in the eastern regions. The opposite pattern occurs for DRO_SEV (Figure 3d) where the eastern regions have higher (lower) probabilities for smaller (larger) values than occurred in the central and western regions. All of the regions exhibit a peak probability for DRO_SEV between 3 and 5; however, the central and western regions have higher probabilities for the most severe droughts (DRO_SEV > 12), leading to larger average DRO_SEV in those regions. Because regional differences are largest for the FD_INT term, differences in the rate of intensification strongly influence the FDII distributions, with the eastern regions having the largest average FDII (Figure 3b). However, inclusion of the DRO_SEV term flattens the distributions and shifts them to the right by decreasing (increasing) the probabilities for smaller (larger) FDII. Finally, for each variable, the distributions and average values for the central regions lie between those for the western and eastern regions, suggesting that their location within a climate transition zone leads to a blending of flash drought intensification and severity characteristics.

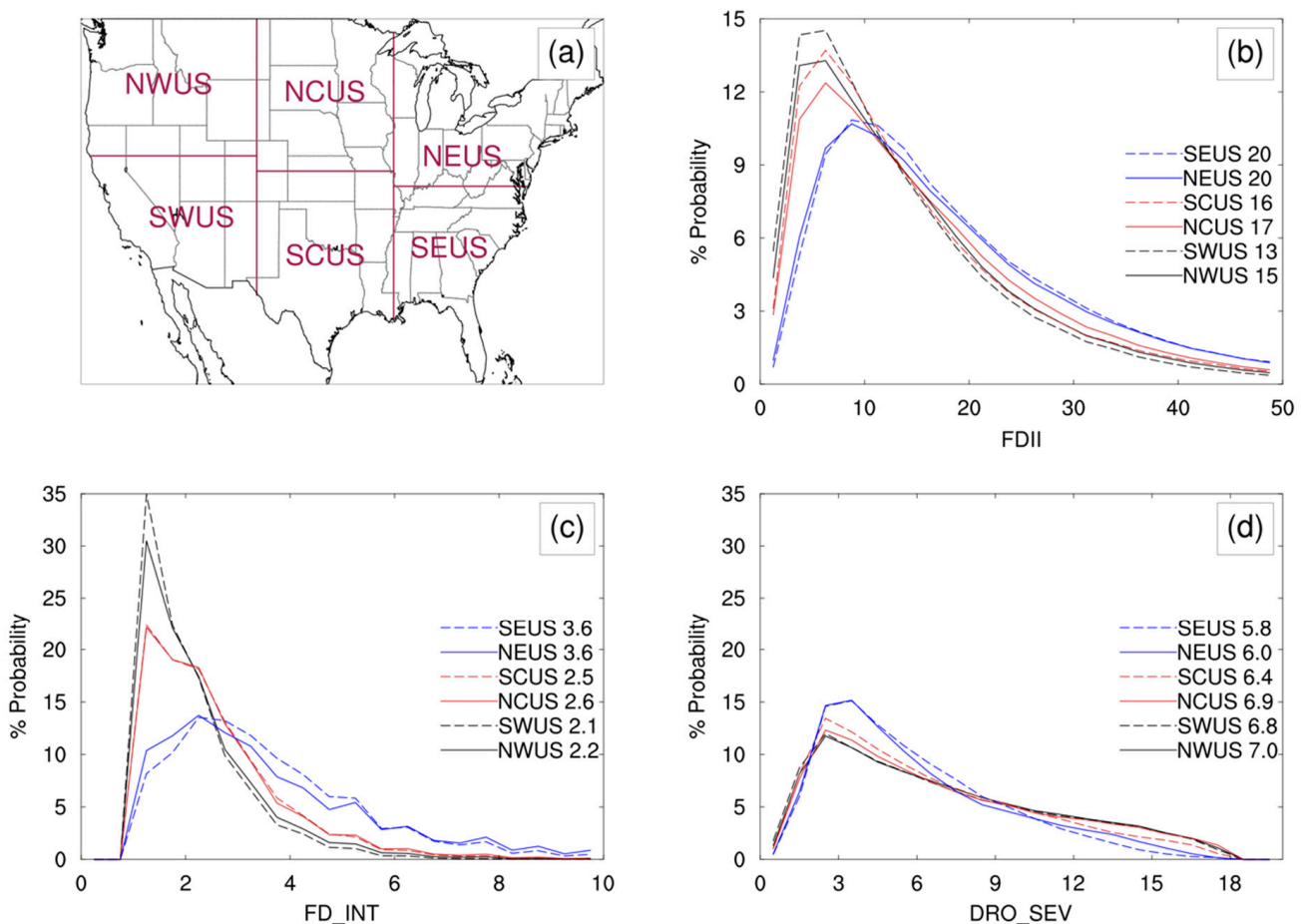


Figure 3. (a) Map showing the six regions that were used to compute probability density functions for (b) FDII, (c) FD_INT, and (d) DRO_SEV using pentad data from April–October during 1979–2017. The mean value for each regional distribution is also shown on each panel. The distributions and mean values were computed using data from individual pentads and grid points for which flash drought occurred.

The relationship between FD_INT and DRO_SEV in each region is examined more closely using the scatterplots shown in Figure 4. The data points represent spatial averages for each pentad containing flash drought somewhere within a given region, with values at grid points without flash drought set to zero prior to computing the averages. Including all grid points in the averages allows us to explore regional-scale relationships between these terms; however, it is important to note that the strength of these relationships may vary for individual grid points due to local soil, vegetation, and climate properties that influence their susceptibility to flash drought. Figure 4 also shows linear regression statistics for each region. Significance testing with $\alpha = 0.05$ showed that the correlation between DRO_SEV and FD_INT is significant in each of the regions.

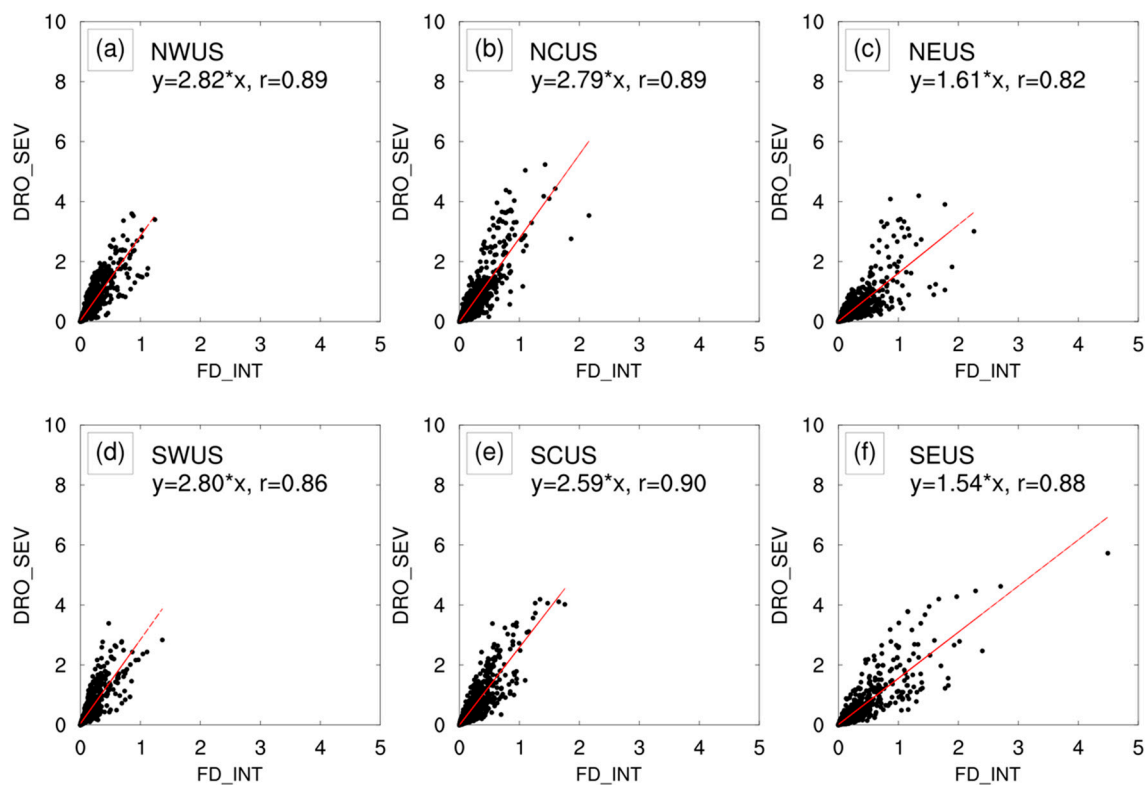


Figure 4. Scatterplot showing the relationship between the FD_INT and DRO_SEV terms for the (a) northwestern US, (b) north-central US, (c) northeastern US, (d) southwestern US, (e) south-central US, and (f) southeastern US regions shown in Figure 3a. The points represent spatial averages computed using data from each pentad for which flash drought occurred somewhere within a given region during April–October from 1979–2017. The red lines show the linear least squares fit for each region, with the slope of the regression and the Pearson correlation coefficient shown at the top of each panel.

Overall, it is evident that the FD_INT and DRO_SEV terms are strongly correlated, with Pearson correlation coefficients between 0.82 and 0.90. The strong relationship between FD_INT and DRO_SEV when assessed at regional scales indicates that the magnitude of rapid intensification is closely tied to the subsequent drought severity when flash drought occurs. This result is consistent with studies by Otkin et al. (2014, 2015) [6,37] that showed that locations experiencing rapid increases in moisture stress are also more likely to experience severe drought than are areas characterized by slower intensification. This suggests that physical processes such as land–atmosphere coupling and atmospheric blocking that have been shown to initiate flash drought [56,59–61] also produce a more favorable environment for drought persistence. It could also indicate that more rapid intensification leads to drier soils that take longer to return to the DRO_BASE threshold once conditions begin to improve. Another notable feature is that the linear regressions for the western and central regions are much steeper than those for the eastern regions, which

shows that a similar rate of intensification in those regions is more likely to lead to severe drought conditions. These regional differences are indicative of the tendency for drought conditions to persist longer in the western US where precipitation is less reliable, and in the central US where strong land–atmosphere feedbacks [54,56] could potentially lead to a higher likelihood of drought persistence following a period of rapid intensification.

3.2. Flash Drought Case Study

In this section, we assess the congruence between the FD_INT, DRO_SEV, and FDII and various datasets capturing the impacts of the 2012 flash drought on prime agricultural lands in the United States. Figure 5 shows maps of the maximum FD_INT, DRO_SEV, and FDII that occurred between 1 May and 18 August 2012, along with the USDM drought analysis and topsoil moisture, corn, and soybean condition anomalies on 18 August 2012, and annual yield departures for corn and soybeans at the end of the growing season. The USDM is generated each week through expert synthesis of multiple data sources to classify conditions into one of six categories ranging from no drought to abnormally dry (D0) and moderate (D1), severe (D2), extreme (D3), and exceptional (D4) drought [33]. The impact of the flash drought on corn and soybean yields is assessed using county-level estimates from the US Department of Agriculture’s National Agricultural Statistics Service (NASS) Quickstats database (<http://quickstats.nass.usda.gov>; accessed on 1 February 2021). Trend-adjusted percentage yield departures were computed for each county and crop after fitting a linear regression to the corresponding yield time series from 2000–2019 to account for local changes over time. Corn, soybean, and topsoil moisture condition data at county scale were also obtained from NASS. These datasets are based on surveys from local experts knowledgeable in visually identifying crop and soil moisture conditions [11]. Crop conditions are reported in five categories ranging from very poor to excellent, whereas topsoil moisture is reported in four categories ranging from very short to surplus. Crop and soil moisture anomalies were computed for 18 August 2012 by subtracting the mean conditions for that week based on the period of record.

FDII and component patterns in Figure 5 indicate that flash drought conditions occurred across most of the central and Midwestern US during 2012. The largest FD_INT values are concentrated in the eastern half of the region (Figure 5a). In contrast, very large values of DRO_SEV are found across a much more extensive area (Figure 5b), similar to the widespread severe-to-exceptional drought conditions depicted by the USDM (Figure 5d). The tendency for larger FD_INT in the eastern US and larger DRO_SEV across both the central and eastern US during this event is consistent with the east-to-west transition in flash drought characteristics shown in the climatological analyses (Figure 2). Comparison of the FDII (Figure 5c) and FD_INT (Figure 5a) maps shows that inclusion of the DRO_SEV term in the FDII led to a notable westward expansion of areas characterized by severe drought. The more expansive depiction of severe drought conditions by the FDII aligns more closely with areas containing substantial crop yield losses (Figure 5e,f) and negative soil and crop condition anomalies (Figure 5g–i). For example, very dry topsoil and poor crop conditions extended from Ohio westward across the entire Corn Belt and into the High Plains. Corn and soybean yields were at least 25% below the long-term trend in most counties in this region. Though the entire area experienced flash drought, FD_INT by itself was unable to capture the westward extent of the most severe impacts on the land surface and agriculture as depicted by the FDII.

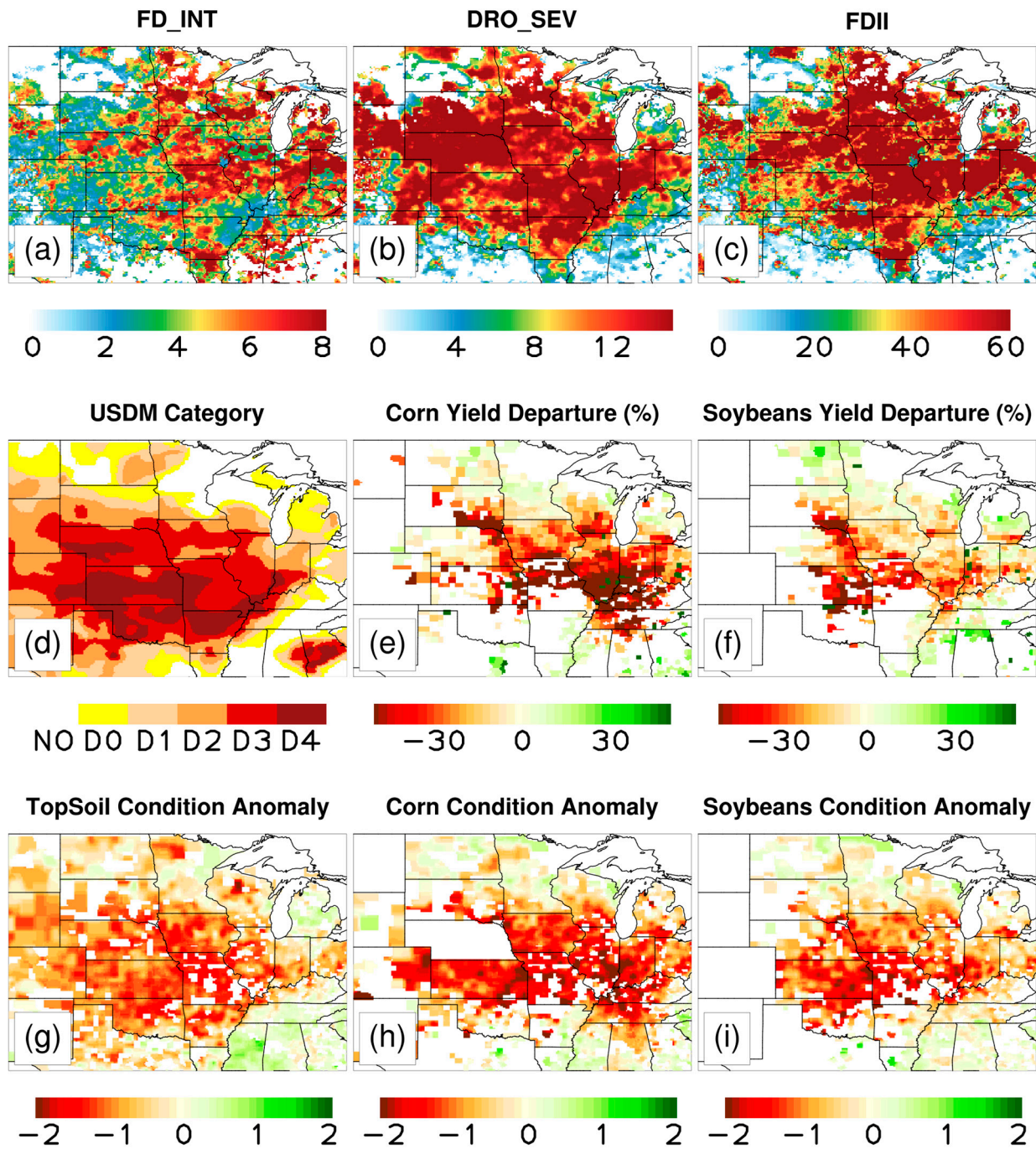


Figure 5. Maximum (a) FD_INT, (b) DRO_SEV, and (c) FDII values for each grid point between 1 May and 18 August 2012. (d) USDM drought analysis on 18 August 2012. Trend-adjusted yield departures (%) for 2012 for (e) corn and (f) soybeans. Anomalies in NASS (g) topsoil moisture, (h) corn, and (i) soybean conditions on 18 August 2012.

To more closely examine relationships between the FDII and crop variables, Figure 6 shows correlations computed using data from the region shown in Figure 5. Significance testing was performed for each variable pair using an equivalent sample size to account for potential autocorrelation between the variables and differences in the number of non-missing points in each variable. All of the correlations were found to be statistically significant at the $\alpha = 0.05$ confidence level. Overall, it is evident that strong correlations exist between most of these variables. For the USDM, crop condition, and crop yield variables, the correlations are strongest for DRO_SEV and FDII and slightly weaker for

August and September [63]). In contrast, the 18-pentad time period used to compute the DRO_SEV overlapped with these critical stages in 2012 (not shown). Second, because the rapid drought intensification occurred early in the growing season, it quickly set the stage for extreme drought conditions to be present during a much longer portion of the growing season and therefore provide the potential for the drought to exert a larger impact on crop yields. Indeed, without the “flash” part of the 2012 drought, crop yields likely would have been higher even if extreme drought conditions had still developed later in the growing season simply because the crops would have experienced less time in drought. Thus, this case study demonstrates that both the unusually rapid rate of intensification and the resultant drought severity should be considered within an FDII framework when evaluating flash drought characteristics and their impacts on land–surface conditions.

4. Discussion

This study presents a new flash drought monitoring framework that explicitly accounts for both the rapid rate of intensification and the resultant drought severity when assessing the intensity of flash drought. By including both components, the FDII provides a more comprehensive measure of flash drought severity than existing methods that do not consider the severity or longevity of the drought after the period of rapid intensification ends. This is an important consideration because an event in which an initial period of rapid intensification transitions into severe and long-lasting drought conditions will have a larger impact on vegetation health, crop yields, ecosystems, and water resources than would an event with the same magnitude of rapid intensification that does not lead to sustained drought.

The FDII framework was demonstrated using 0–40 cm soil moisture percentiles from the Noah land surface model from 1979–2017. The FDII was computed as the product of two terms measuring the maximum rate of intensification (FD_INT) and average drought severity (DRO_SEV) relative to a set of thresholds representing the minimum requirements for flash drought. Overall, the study revealed large regional differences in flash drought characteristics across the US. For example, FD_INT was larger on average across the eastern US whereas DRO_SEV was larger over the central and western US where long-term drought conditions are more likely due to higher evaporative demand and less reliable rainfall. The larger DRO_SEV meant that the average strength of flash droughts across the western and central US was greater than would otherwise be apparent if only the magnitude of the rapid intensification was used to represent their intensity. Analysis of the 2012 US flash drought showed that the FDII depiction of severe drought conditions aligned more closely with regions containing poor crop conditions and large yield losses than occurred when using the intensification rate component (FD_INT) in isolation. Together, the case study and climatology illustrate why it is important to consider both the magnitude of the rapid intensification and the resultant drought severity when assessing the strength of flash drought events. Comparison of the FD_INT and DRO_SEV terms also showed that they are strongly correlated to each other at regional scales, which indicates that the subsequent drought severity is closely related to the magnitude of the preceding period of rapid intensification.

While the FDII formula presented in this study demonstrates the merit of a combined intensification rate and severity framework for describing flash drought, future work will explore the utility of other formulations. Here, a percentile-based approach was used to compute the FDII because such methods have been widely employed during previous studies to identify flash drought. Though percentile-based methods have proven useful for this purpose, an important limitation is that they convert an unbounded nonlinear distribution of standardized anomalies into a bounded linear distribution of percentiles. This limitation could potentially be mitigated by using nonlinear functions in the FD_INT and DRO_SEV terms so that additional weight is given to more extreme events. Such modifications could be especially important for flash drought because the rapid temporal changes that occur during these events are located in the tail of the distribution where

large changes in standardized anomalies for a variable may only lead to small changes in percentile space. It is also challenging to apply percentile-based methods to datasets with short periods of record because there is insufficient data to represent the distribution. For example, even with 40 years of data, there are only enough data points to resolve the distribution at 2.5 percentile intervals.

Though percentiles are more intuitive and easier to communicate to the general public, it may be advantageous to use standardized anomalies because their unbounded range of values can more accurately represent the magnitude of extreme events in datasets with shorter periods of record. This is because standardized anomalies are computed using a theoretical continuous distribution whereas percentiles are generated using a discrete set of historical events. An FDII formula that employs standardized change anomalies could be patterned off the rapid change index developed by Otkin et al. (2014, 2015) [6,37] that represents the accumulated magnitude of rapid changes in a variable over some period of time. Modifying the rapid change index so that it also includes a drought severity component would make it consistent with the FDII framework.

Additional studies are necessary to investigate the physical drivers of flash drought such as land–atmosphere coupling, remote teleconnections, and blocking anticyclones, and determine how these processes influence the magnitude of the rapid intensification and drought severity terms that comprise the FDII. A deeper understanding of these processes and how they may vary for different regions and seasons would aid efforts to not only predict flash drought occurrence but also its intensity. It would also be beneficial to use the FDII and its components to examine flash drought characteristics in other parts of the world with climate types that do not occur in the contiguous US, as well as to examine their spatial heterogeneity using methods such as the Gini index [64]. Such information could be used to perform vulnerability assessments to better understand the exposure, sensitivity, and adaptive capacity of different groups to flash drought. Finally, the FDII framework could be applied to other drought monitoring variables such as evaporative demand and evapotranspiration to assess the compound nature and cascading impacts of flash drought on the environment because no single dataset can represent all aspects of flash drought by itself. This could be done both in retrospective studies and as part of real-time monitoring systems. These and other topics will be explored in future studies.

Author Contributions: Conceptualization, J.A.O., Y.Z., E.D.H., H.N., M.C.W. and A.H.; methodology, J.A.O. and Y.Z.; software, Y.Z.; validation, J.A.O. and Y.Z.; formal analysis, Y.Z. and J.A.O.; investigation, Y.Z. and J.A.O.; resources, J.A.O.; data curation, Y.Z.; writing—original draft preparation, J.A.O.; writing—review and editing, J.A.O., Y.Z., E.D.H., J.I.C., J.B.B., H.N., M.C.W., T.W.F., A.H., M.S. and M.C.A.; visualization, J.A.O. and Y.Z.; supervision, J.A.O. and E.D.H.; funding acquisition, J.A.O., E.D.H. and J.B.B. All authors have read and agreed to the published version of the manuscript.

Funding: This research was funded by the National Aeronautics and Space Administration (NASA) Water Resources Program, grant #80NSSC19K1266 and by the NASA Land Cover and Land Use Change (LCLUC) Program, grant #80NSSC18K0483. JBB and JIC were also supported by the National Science Foundation, grant #OIA-1946093. HN was supported by the Northern Australia Climate Program funded by Meat and Livestock Australia, the Queensland Government, and the University of Southern Queensland.

Institutional Review Board Statement: Not applicable.

Informed Consent Statement: Not applicable.

Data Availability Statement: Data used in this study is available upon request.

Acknowledgments: We thank three anonymous reviewers for their comments and questions that helped improve the quality of the manuscript.

Conflicts of Interest: The authors declare no conflict of interest. The funders had no role in the design of the study; in the collection, analyses, or interpretation of data; in the writing of the manuscript, or in the decision to publish the results.

References

1. Otkin, J.A.; Svoboda, M.; Hunt, E.D.; Ford, T.W.; Anderson, M.C.; Hain, C.; Basara, J.B. Flash Droughts: A Review and Assessment of the Challenges Imposed by Rapid-Onset Droughts in the United States. *Bull. Am. Meteorol. Soc.* **2018**, *99*, 911–919. [CrossRef]
2. Otkin, J.A.; Anderson, M.C.; Hain, C.; Mladenova, I.; Basara, J.; Svoboda, M. Examining flash drought development using the thermal infrared based Evaporative Stress Index. *J. Hydrometeorol.* **2013**, *14*, 1057–1074. [CrossRef]
3. Ford, T.W.; Labosier, C.F. Meteorological conditions associated with the onset of flash drought in the eastern United States. *Agric. For. Meteorol.* **2017**, *247*, 414–423. [CrossRef]
4. Anderson, M.C.; Hain, C.; Otkin, J.A.; Zhan, X.; Mo, K.; Svoboda, M.; Wardlow, B.; Pimstein, A. An intercomparison of drought indicators based on thermal remote sensing and NLDAS simulations with U.S. Drought Monitor Classifications. *J. Hydrometeorol.* **2013**, *14*, 1035–1056. [CrossRef]
5. Mozny, M.; Trnka, M.; Zalud, Z.; Hlavinka, P.; Nekovar, P.; Potop, V.; Virag, M. Use of a soil moisture network for drought monitoring in the Czech Republic. *Theor. Appl. Climatol.* **2012**, *107*, 99–111. [CrossRef]
6. Otkin, J.A.; Anderson, M.C.; Hain, C.; Svoboda, M. Examining the relationship between drought development and rapid changes in the Evaporative Stress Index. *J. Hydrometeorol.* **2014**, *15*, 938–956. [CrossRef]
7. Hunt, E.; Svoboda, M.; Wardlow, B.; Hubbard, K.; Hayes, M.J.; Arkebauer, T. Monitoring the effects of rapid onset of drought on non-irrigated maize with agronomic data and climate-based drought indices. *J. Agric. For. Meteorol.* **2014**, *191*, 1–11. [CrossRef]
8. Ford, T.W.; McRoberts, D.B.; Quiring, S.M.; Hall, R.E. On the utility of in situ soil moisture observations for flash drought early warning in Oklahoma, USA. *Geophys. Res. Lett.* **2015**, *42*, 9790–9798. [CrossRef]
9. Zscheischler, J.; Westra, S.; Hurk, B.J.J.M.V.D.; Seneviratne, S.I.; Ward, P.J.; Pitman, A.; AghaKouchak, A.; Bresch, D.N.; Leonard, M.; Wahl, T.; et al. Future climate risk from compound events. *Nat. Clim. Chang.* **2018**, *8*, 469–477. [CrossRef]
10. Christian, J.I.; Basara, J.B.; Otkin, J.A.; Hunt, E.D. Regional characteristics of flash droughts across the United States. *Environ. Res. Commun.* **2019**, *1*, 125004. [CrossRef]
11. Otkin, J.A.; Anderson, M.C.; Hain, C.; Svoboda, M.; Johnson, D.; Mueller, R.; Tadesse, T.; Wardlow, B.; Brown, J. Assessing the evolution of soil moisture and vegetation conditions during the 2012 United States flash drought. *Agric. For. Meteorol.* **2016**, *218–219*, 230–242. [CrossRef]
12. Anderson, M.C.; Zolin, C.; Sentelhas, P.; Hain, C.R.; Semmens, K.; Yilmaz, M.T.; Gao, F.; Otkin, J.A.; Tetrault, R. Assessing correlations of satellite-derived evapotranspiration, precipitation, and leaf area index anomalies with yields of major Brazilian crops. *Remote Sens. Environ.* **2016**, *174*, 82–99. [CrossRef]
13. Zhang, M.; Yuan, X.; Otkin, J.A. Remote sensing of the impact of flash drought events on terrestrial carbon dynamics over China. *Carbon Balance Manag.* **2020**, *15*, 20. [CrossRef]
14. Case, J.L.; Zavodsky, B.T. Evolution of 2016 drought in the Southeastern United States from a land surface modeling perspective. *Results Phys.* **2018**, *8*, 654–656. [CrossRef]
15. NOAA National Centers for Environmental Information (NCEI) US Billion-Dollar Weather and Climate Disasters. 2017. Available online: <https://www.ncdc.noaa.gov/billions/> (accessed on 1 June 2021).
16. Sternberg, T. Chinese drought, bread and the Arab Spring. *Appl. Geogr.* **2012**, *34*, 519–524. [CrossRef]
17. Otkin, J.A.; Shafer, M.; Svoboda, M.; Wardlow, B.; Anderson, M.C.; Hain, C.; Basara, J. Facilitating the use of drought early warning information through interactions with agricultural stakeholders. *Bull. Am. Meteorol. Soc.* **2015**, *96*, 1073–1078. [CrossRef]
18. Otkin, J.A.; Haigh, T.; Mucia, A.; Anderson, M.C.; Hain, C.R. Comparison of agricultural stakeholder survey results and drought monitoring datasets during the 2016 US Northern Plains flash drought. *Weather Clim. Soc.* **2018**, *10*, 867–883. [CrossRef]
19. Otkin, J.A.; Zhong, Y.; Hunt, E.D.; Basara, J.; Svoboda, M.; Anderson, M.C.; Hain, C. Assessing the evolution of soil moisture and vegetation conditions during a flash drought—flash recovery sequence over the south-central United States. *J. Hydrometeorol.* **2019**, *20*, 549–562. [CrossRef]
20. Haigh, T.R.; Otkin, J.A.; Mucia, A.; Hayes, M.; Burbach, M. When do livestock producers’ take action during drought? How environmental cues, climate information resources, and adaptive capacity shape response. *Adv. Meteorol.* **2019**. [CrossRef]
21. Nguyen, H.; Wheeler, M.C.; Otkin, J.A.; Cowan, T.; Frost, A.; Stone, R. Using the evaporative stress index to monitor flash drought in Australia. *Environ. Res. Lett.* **2019**, *14*. [CrossRef]
22. Basara, J.B.; Christian, J.I.; Wakefield, R.A.; Otkin, J.A.; Hunt, E.H.; Brown, D.P. The evolution, propagation, and spread of flash drought in the Central United States during 2012. *Environ. Res. Lett.* **2019**, *14*. [CrossRef]
23. Christian, J.I.; Basara, J.B.; Hunt, E.D.; Otkin, J.A.; Xiao, X. Flash drought development and cascading impacts associated with the 2010 Russian heatwave. *Environ. Res. Lett.* **2020**, *15*, 094078. [CrossRef]
24. Liu, Y.; Zhu, Y.; Ren, L.; Otkin, J.A.; Hunt, E.D.; Yang, X.; Yuan, F.; Jian, S. Two different methods for flash drought identification: Comparison of their strengths and limitations. *J. Hydrometeorol.* **2020**, *21*, 691–704. [CrossRef]
25. Christian, J.I.; Basara, J.B.; Otkin, J.A.; Hunt, E.D.; Wakefield, R.A.; Flanagan, P.X.; Xiao, X. A methodology for flash drought identification: Application of flash drought frequency across the United States. *J. Hydrometeorol.* **2019**, *20*, 833–846. [CrossRef]
26. Li, J.; Wang, Z.; Wu, X.; Chen, J.; Guo, S.; Zhang, Z. A new framework for tracking flash drought events in space and time. *Catena* **2020**, *194*, 104763. [CrossRef]
27. Koster, R.D.; Schubert, S.D.; Wang, H.; Mahanama, S.P.; Deangelis, A.M. Flash drought as captured by reanalysis data: Disentangling the contributions of precipitation deficit and excess evapotranspiration. *J. Hydrometeorol.* **2019**, *20*, 1241–1258. [CrossRef]

28. Liu, Y.; Zhu, Y.; Zhang, L.; Ren, L.; Yuan, F.; Yang, X.; Jiang, S. Flash droughts characterization over China: From a perspective of the rapid intensification rate. *Sci. Total Environ.* **2020**, *704*, 135373. [[CrossRef](#)]
29. Osman, M.; Zaitchik, B.F.; Badr, H.S.; Christian, J.I.; Tadesse, T.; Otkin, J.A.; Anderson, M.C. Flash drought onset over the Contiguous United States: Sensitivity of inventories and trends to quantitative definitions. *Hydrol. Earth Syst. Sci.* **2021**, *25*, 565–581. [[CrossRef](#)]
30. Hobbins, M.T.; Wood, A.; McEvoy, D.; Huntington, J.; Morton, C.; Anderson, M.C.; Hain, C. The Evaporative Demand Drought Index: Part I—Linking drought evolution to variations in evaporative demand. *J. Hydrometeorol.* **2016**, *17*, 1745–1761. [[CrossRef](#)]
31. McEvoy, D.J.; Huntington, J.L.; Hobbins, M.T.; Wood, A.; Morton, C.; Anderson, M.C.; Hain, C. The Evaporative Demand Drought Index. Part II: CONUS-wide assessment against common drought indicators. *J. Hydrometeorol.* **2016**, *17*, 1763–1779. [[CrossRef](#)]
32. Noguera, I.; Domínguez-Castro, F.; Vicente-Serrano, S.M. Characteristics and trends of flash droughts in Spain, 1961–2018. *Ann. N. Y. Acad. Sci.* **2020**, *1472*, 155–172. [[CrossRef](#)] [[PubMed](#)]
33. Svoboda, M.; LeComte, D.; Hayes, M.; Heim, R.; Gleason, K.; Angel, J.; Rippey, B.; Tinker, R.; Palecki, M.; Stooksbury, D.; et al. The Drought Monitor. *Bull. Am. Meteorol. Soc.* **2002**, *83*, 1181–1190. [[CrossRef](#)]
34. Chen, L.G.; Gottschalck, J.; Hartman, A.; Miskus, D.; Tinker, R.; Artusa, A. Flash Drought Characteristics Based on US Drought Monitor. *Atmosphere* **2019**, *10*, 498. [[CrossRef](#)]
35. Pendergrass, A.G.; Meehl, G.A.; Pulwarty, R.; Hobbins, M.; Hoell, A.; AghaKouchak, A.; Bonfils, C.J.W.; Gallant, A.J.E.; Hoerling, M.; Hoffmann, D.; et al. Flash droughts present a new challenge for subseasonal-to-seasonal prediction. *Nat. Clim. Chang.* **2020**, *10*, 191–199. [[CrossRef](#)]
36. Lisonbee, J.; Woloszyn, M.; Skumanich, M. Making sense of flash drought: Definitions, indicators, and where we go from here. *J. Appl. Serv. Climatol.* **2021**. [[CrossRef](#)]
37. Otkin, J.A.; Anderson, M.C.; Hain, C.; Svoboda, M. Using temporal changes in drought indices to generate probabilistic drought intensification forecasts. *J. Hydrometeorol.* **2015**, *16*, 88–105. [[CrossRef](#)]
38. Hoell, A.; Parker, B.-A.; Downey, M.; Umphlett, N.; Jencso, K.; Akyuz, F.A.; Peck, D.; Hadwen, T.; Fuchs, B.; Kluck, D.; et al. Lessons learned from the 2017 flash drought across the US Northern Great Plains and Canadian Prairies. *Bull. Am. Meteorol. Soc.* **2020**, *101*, E2171–E2185. [[CrossRef](#)]
39. McNeeley, S.M.; Beeton, T.A.; Ojima, D.S. Drought risk and adaptation in the interior United States: Understanding the importance of local context for resource management in times of drought. *Weather Clim. Soc.* **2016**, *8*, 147–161. [[CrossRef](#)]
40. Ummerhofer, C.C.; Meehl, G.A. Extreme weather and climate events with ecological relevance: A review. *Philos. Trans. R. Soc. B* **2018**, *8*, 372. [[CrossRef](#)]
41. Walsh, J.E.; Ballinger, T.J.; Euskirchen, E.S.; Hanna, E.; Mard, J.; Overland, J.E.; Tangen, H.; Vihma, T. Extreme weather and climate events in northern areas: A review. *Earth-Sci. Rev.* **2020**, *209*. [[CrossRef](#)]
42. Ojima, D.S.; Conant, R.T.; Parton, W.J.; Lockett, J.M.; Even, T.L. Recent climate changes across the Great Plains and implications for natural resource management practices. *Rangel. Ecol. Manag.* **2021**, in press. [[CrossRef](#)]
43. Yuan, X.; Wang, L.; Wu, P.; Ji, P.; Sheffield, J.; Zhang, M. Anthropogenic shift towards higher risk of flash drought over China. *Nat. Commun.* **2019**, *10*, 4661. [[CrossRef](#)]
44. Driouechi, F.; Elrhaz, K.; Moufouma-Okia, W.; Aridal, K.; Balhane, S. Assessing future changes of climate extreme events in the CORDEX-MENA region using regional climate model ALADIN-Climate. *Earth Syst. Environ.* **2020**, *4*, 477–492. [[CrossRef](#)]
45. Cutter, S.L.; Boruff, B.J.; Shirley, W.L. Social vulnerability to environmental hazards. *Soc. Sci. Q.* **2003**. [[CrossRef](#)]
46. Tánago, I.G.; Urquijo, J.; Blauhut, V.; Villarroya, F.; De Stefano, L. Learning from experience: A systematic review of vulnerability to drought. *Nat. Hazards* **2016**, *80*, 951–973. [[CrossRef](#)]
47. Engstrom, J.; Jafarzadegan, K.; Moradkhani, H. Drought vulnerability in the United States: An integrated assessment. *Water* **2020**, *12*, 2033. [[CrossRef](#)]
48. Singh, N.P.; Bantilan, C.; Byjesh, K. Vulnerability and policy relevance to drought in the semi-arid tropics of Asia—A retrospective analysis. *Weather Clim. Extrem.* **2014**, *3*, 54–61. [[CrossRef](#)]
49. Weis, S.W.M.; Agostini, V.N.; Roth, L.M.; Gilmer, B.; Schill, S.R.; Knowles, J.E.; Blyther, R. Assessing vulnerability: An integrated approach for mapping adaptive capacity, sensitivity, and exposure. *Clim. Chang.* **2016**, *136*, 615–629. [[CrossRef](#)]
50. Anderson, C.C.; Hagenlocher, M.; Renaud, F.G.; Sebesvari, Z.; Cutter, S.L.; Emrich, C.T. Comparing index-based vulnerability assessments in the Mississippi Delta: Implications of contrasting theories, indicators, and aggregation methodologies. *Int. J. Disaster Risk Reduct.* **2019**, *39*, 101128. [[CrossRef](#)]
51. Wei, H.; Xia, Y.; Mitchell, K.E.; Ek, M.B. Improvement of the Noah land surface model for warm season processes: Evaluation of water and energy flux simulation. *Hydrol. Process.* **2013**, *27*, 297–303. [[CrossRef](#)]
52. Xia, Y.; Mitchell, K.; Ek, M.; Sheffield, J.; Cosgrove, B.; Wood, E.; Luo, L.; Alonge, C.; Wei, H.; Meng, J.; et al. Continental-scale water and energy flux analysis and validation of the North American Land Data Assimilation System project phase 2 (NLDAS-2): 1. Intercomparison and application of model products. *J. Geophys. Res.* **2012**, *117*, D03110. [[CrossRef](#)]
53. Ford, T.W.; Quiring, S. Comparison of contemporary in situ, model, and satellite remote sensing soil moisture with a focus on drought monitoring. *Water Resour. Res.* **2019**, *55*, 1565–1582. [[CrossRef](#)]
54. Koster, R.D.; Dirmeyer, P.A.; Guo, Z.; Bonan, G.; Chan, E.; Cox, P.; Gordon, C.T.; Kanae, S.; Kowalczyk, E.; Lawrence, D.; et al. Regions of strong coupling between soil moisture and precipitation. *Science* **2004**, *305*, 1138–1140. [[CrossRef](#)]
55. Dirmeyer, P. The terrestrial segment of soil moisture–climate coupling. *Geophys. Res. Lett.* **2011**, *38*. [[CrossRef](#)]

56. Basara, J.B.; Christian, J.I. Seasonal and interannual variability of land–atmosphere coupling across the Southern Great Plains of North America using the North American regional reanalysis. *Int. J. Climatol.* **2018**, *38*, 964–978. [[CrossRef](#)]
57. Wakefield, R.A.; Basara, J.B.; Furtado, J.C.; Illston, B.G.; Ferguson, C.R.; Klein, P.M. A modified framework for quantifying land-atmosphere covariability during hydrometeorological and soil wetness extremes in Oklahoma. *J. Appl. Meteorol. Climatol.* **2019**, *58*, 1465–1483. [[CrossRef](#)]
58. Zhong, Y.; Otkin, J.A.; Anderson, M.C.; Hain, C.R. Observational assessment of the relationship between the Evaporative Stress Index and soil moisture and temperature across the United States. *J. Hydrometeorol.* **2020**, *21*, 1469–1484. [[CrossRef](#)]
59. Hoerling, M.; Eischeid, J.K.; Kumar, A.J.; Leung, R.; A Mariotti, A.W.; Mo, K.; Schubert, S.D.; Seager, R. Causes and predictability of the 2012 Great Plains drought. *Bull. Am. Meteorol. Soc.* **2014**, *95*, 269–282. [[CrossRef](#)]
60. Gerken, T.; Bromley, G.T.; Ruddell, B.L.; Williams, S.; Stoy, P.C. Convective suppression before and during the United States Northern Great Plains flash drought of 2017. *Hydrol. Earth Syst. Sci.* **2018**, *22*, 4155–4163. [[CrossRef](#)]
61. DeAngelis, A.M.; Wang, H.; Koster, R.D.; Schubert, S.D.; Chang, Y.; Marshark, J. Prediction skill of the 2012 US Great Plains flash drought in Subseasonal Experiment (SubX) Models. *J. Clim.* **2020**, *33*, 6229–6253. [[CrossRef](#)]
62. Lobell, D.B.; Roberts, M.J.; Schlenker, W.; Braun, N.; Little, B.B.; Rejesus, R.M.; Hammer, G. Greater sensitivity of drought accompanies maize yield increase in the US Midwest. *Science* **2014**, *344*, 516–519. [[CrossRef](#)] [[PubMed](#)]
63. Mishra, V.; Cherkauer, K. Retrospective droughts in the crop growing season: Implications to corn and soybean yield in the Midwestern United States. *Agric. For. Meteorol.* **2010**, *150*, 1030–1045. [[CrossRef](#)]
64. Gini, C. Measurement of inequality of incomes. *Econ. J.* **1921**, *31*, 124–126. [[CrossRef](#)]